Japanese Journal of Applied Physics **50** (2011) 01AF05 **REGULAR PAPER**
**DOI:** 10.1143/JJAP.50.01AF05

# Magnetoelectronic and Optical Properties of Monolayer and AB-Stacked Bilayer Graphenes

Yen-Hung Ho[1], Yu-Huang Chiu[2], Jei Wang[2], De-Hone Lin[1], and Ming-Fa Lin[2*]

[1]*Department of Physics, National Sun Yat-Sen University, Kaohsiung 804, Taiwan*
[2]*Department of Physics, National Cheng Kung University, Tainan 701, Taiwan*

Received April 30, 2010; accepted September 19, 2010; published online January 20, 2011

The low-frequency magneto-absorption spectra of monolayer and bilayer graphene are evaluated within the gradient approximation. On the basis of Peierls tight-binding model, we can draw the wave function distribution over its sublattices and bring them into the calculation of optical spectra. The optical selection rules and the absorption rate can be accurately determined. The interlayer interactions in bilayers effectively alter the Landau level structures and thus the absorption spectra, such as the field dependence of absorption lines and the appearance of double-peaked absorptions. © 2011 The Japan Society of Applied Physics

## 1. Introduction

Few-layer graphenes have attracted considerable experimental and theoretical interests in the past few years since they were experimentally achieved through the mechanical exfoliation from bulk graphite[1)] and the epitaxial growth on silicon carbide.[2)] They are ideal materials to explore the quantum phenomena in two-dimensional electron systems. The hexagonal crystal structure of graphene results in the linear and isotropic energy dispersions intersecting right at the Fermi level $E_F = 0$. With regard to the AB-stacked (Bernal) bilayer graphene, the coupling between layers substantially converts the linear bands into parabolic bands, and lift the symmetry between valence and conduction bands.[3,4)] These subband characteristics can be directly observed through the angular-resolved photoemission spectroscopy, which is capable of identifying the layer number and the stacking consequences.[3,4)] Moreover, a perpendicular magnetic field $B_0\hat{z}$ can effectively quantize the planar electronic states into dispersionless Landau levels. Such Landau quantization brings about more pronounced spectral features than those at zero field, which gives rise to a better understanding of intrinsic physical properties. These energy levels can be examined through the measurements of quantum Hall conductivity,[5–10)] scanning tunneling spectroscopy,[11)] and cyclotron resonance.[12–16)] In this work, the Landau levels and their optical responses are numerically investigated for monolayer and bilayer graphene. Both the effect of interlayer interactions and field strength are examined in detail.

The characteristics of zero-field subbands should be directly reflected in the discrete Landau levels. Owing to the linear bands at zero field, monolayer Landau levels are close to be square-root dependent on field. In particular, one of them is located right at the charge neutrality point. With regard to bilayer graphene, Landau levels derived from parabolic bands are close to be linearly $B_0$-dependent. In the theoretical aspect, previous works are mainly based on the effective-mass model[17,18)] and the Peierls tight-binding model.[19–22)] The former is a kind of approximation method with respect to the Fermi-momentum states ($K$-point), Only the interlayer interaction $\gamma_1$ is taken into account and treated as perturbations. This simplified model can properly evaluate the linear-band associated Landau levels in monolayers and the parabolic-band associated levels in bilayers. Nevertheless, it is not suitable for higher Landau levels since the actual zero-field subbands would gradually deviate from the ideal linear or parabolic dispersions with the increment of state energy.

In the present study, the Peierls tight-binding model is utilized to study the magnetoelectronic properties of graphene layers.[19–22)] The calculation can conveniently take account of all interlayer interactions and field-induced Peierls phase simultaneously. Accordingly, the numerical results are relatively reliable over a much wider energy range. In bilayer graphene, the breakdown of electron–hole symmetry are obtained, as well as the appearance of field-dependent energy gap. In addition, how the wave function distributed over the constituent sublattices is also accessible in this model. It enable to clearly define the level indices, and more importantly, provide an intuitive way to investigate the optical transitions between Landau levels. The optical spectra are studied within the gradient approximation. Both the optical selection rules and the absorption rates can be explicitly resolved in response to photon energy and field strength. In bilayers, the interlayer interactions remarkably introduce additional spectral structures. The field evolution of absorption lines closely related to hopping integrals. And the subband asymmetry appears as the double-peaked absorptions. The calculated results would be practical in identifying the magneto-optical measurements on graphene layers.[12–16)] Some spectral features are verified to be in agreement with the experimental results.[8,10–13)]

## 2. Peierls Tight-Binding Model

To begin with, the graphene geometry and its Peierls tight-binding Hamiltonian at $B_0 \neq 0$ are briefly reviewed in ref. 22. In the presence of magnetic field $\boldsymbol{B} = B_0\hat{z}$, the vector potential $\boldsymbol{A} = (0, B_0x, 0)$ makes the Peierls phase $\Delta G(\boldsymbol{R}_j^l, \boldsymbol{R}_k^{l'}) = \int_0^1 (\boldsymbol{R}_k^{l'} - \boldsymbol{R}_j^l) \cdot \boldsymbol{A}[\boldsymbol{R}_j^l + \lambda(\boldsymbol{R}_k^{l'} - \boldsymbol{R}_j^l)]\, d\lambda$ accumulates in the Bloch wave functions.[19–23)] Meanwhile, the Hamiltonian matrix element is expressed as

$$\langle k^{l'}|H|j^l\rangle = \gamma_s(\boldsymbol{R}_j^l, \boldsymbol{R}_k^{l'}) \sum \exp\left[ i\boldsymbol{k} \cdot (\boldsymbol{R}_j^l - \boldsymbol{R}_k^{l'}) + i\frac{e}{\hbar}\Delta G(\boldsymbol{R}_j^l, \boldsymbol{R}_k^{l'})\right] \quad (1)$$

$\boldsymbol{R}_j^l$ ($\boldsymbol{R}_k^{l'}$) stands for the position vector of atom $j$ ($k$) on layer $l$ ($l'$). $\gamma_s(\boldsymbol{R}_j^l, \boldsymbol{R}_k^{l'})$ contains information about the relative atomic hoppings between atoms.[24,25)] The in-plane interactions are

*E-mail address: mflin@mail.ncku.edu.tw

the hopping between inequivalent $A$ and $B$ atoms, $\gamma_0 = -3.12\,\mathrm{eV}$. As to the bilayer graphene, interlayer hoppings are further considered, including $\gamma_1 = 0.38\,\mathrm{eV}$, $\gamma_3 = 0.28\,\mathrm{eV}$, $\gamma_4 = 0.12\,\mathrm{eV}$ as well as the site-energy difference between inequivalent $A$ and $B$ atoms $\gamma_6 = 0.016\,\mathrm{eV}$.

At $B_0 = 0$, the primitive unit cell consists of two ($A$ and $B$) and four ($A^1$, $B^1$, $A^2$, $B^2$) atoms respectively for monolayer and bilayer graphene. In the case of $B_0 \neq 0$, the Peierls phase term acts as a path integral of vector potential and introduces an extended periodic boundary condition. Accordingly, the unit cell has to be $2R_B$-times larger and the Hamiltonian turns into a $2R_B \times 2R_B$-times larger square matrix ($R_B = 79000/B_0$). To solve the huge matrix at small $B_0$, we convert the square matrix into the band-like one.[22] In this manner, both the Landau-level energy $E^{\mathrm{c,v}}$ and eigenfunction $\psi^{\mathrm{c,v}}$ can be efficiently resolved, even for the field down to 0.5 T. For each Landau state, wave function can be represented by its constituent sublattices: $A_N$, $B_N$ for monolayers and $A_N^1$, $B_N^1$, $A_N^2$, $B_N^2$ for bilayers ($N = 1$–$2R_B$).

The optical transitions between Landau levels can be realized through the absorption of electromagnetic radiation, which can be directly measured through the use of cyclotron resonance.[12–16] Based on the Fermi golden rule, the efficiency of the photon emission at zero temperature is given by,[26]

$$A(\omega, B_0) \propto \sum_{n,n'} \int_{1\mathrm{st\ BZ}} \frac{dk_x\,dk_y}{(2\pi)^2} |\langle \psi^{\mathrm{c}}(n, B_0)| \frac{\hat{E}\cdot\boldsymbol{P}}{m_{\mathrm{e}}} |\psi^{\mathrm{v}}(n', B_0)\rangle|^2 \times \left\{ \frac{\Gamma}{[\omega - \omega_{n,n'}(B_0)]^2 + \Gamma^2} - \frac{\Gamma}{[\omega + \omega_{n,n'}(B_0)]^2 + \Gamma^2} \right\}. \quad (2)$$

$\Gamma = 1\,\mathrm{meV}$ is the broadening parameter. $\omega_{n,n'}(B_0) = E^{\mathrm{c}}(n, B_0) - E^{\mathrm{v}}(n', B_0)$ is the energy difference between occupied and unoccupied states. The photons carry energy $\omega$ while the polarization is linear and parallel to graphene plane. The velocity matrix elements are evaluated within the gradient approximation $\hat{E}\cdot\boldsymbol{P}/m_{\mathrm{e}} = \partial H/\partial k_{x,y}$, which is suitable for the carbon related nanosystems to interpret the interactions between electrons and photons.[27,28] Also, the wave function available in this work would offer an important insight into the possible excitation channels and corresponding absorption rates.

## 3. Result Discussions

The Landau energies against field strength are plotted in Figs. 1(a) and 1(b) respectively for monolayer and bilayer graphene. Unlike the traditional electron gas of metals, these Landau levels are not equally spaced. In monolayers, Landau energy is a function of level index $n^{\mathrm{c,v}}$ and field strength $B_0$, $E_n^{\mathrm{c,v}} \propto \pm\sqrt{nB_0}$, where $v$ stands for electrons and $c$ for holes. This specific dependence can be ascribed to the Dirac-cone-like energy bands at zero field, where the level spacings correlate to the in-plane hopping integral $\gamma_0$. The particular $n = 0$ level is located right at $E_{\mathrm{F}}$ which is made up of both electron and hole carriers. The valence and conduction states are perfectly symmetric with respect to $E_{\mathrm{F}}$. In higher energy region or at stronger field, Landau levels would gradually deviate from this simple field dependence since the corresponding electronic states at $B_0 = 0$ gradually exceed the linear dispersion relation.

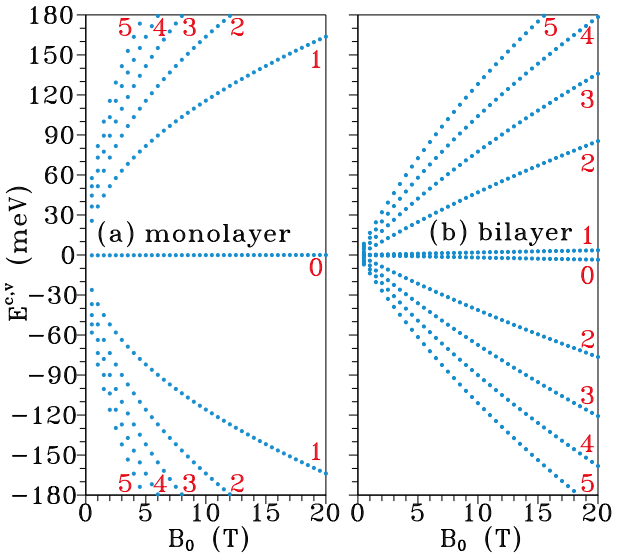


**Fig. 1.** (Color online) Landau levels with quantum index $n^{\mathrm{c,v}} \leq 5$ as a function of magnetic field $B_0$ for (a) monolayer and (b) bilayer Bernal graphene.

In bilayer graphene, the Landau-level distribution is significantly influenced by the interlayer interactions. Those of $n^{\mathrm{c,v}} \leq 5$ are illustrated in Fig. 1(b). The level spacings are evidently closer than those in monolayers. The symmetry between electron and hole states is absent; more specifically, Landau levels are denser in occupied states with compared to unoccupied states. The zero-energy level has split into $n^{\mathrm{c}} = 0$ and $n^{\mathrm{v}} = 1$ that gives rise to a small energy gap. $\gamma_4$ and $\gamma_6$ are responsible for this $B_0$-modulated width. Also, it is noteworthy that the Landau levels converted from the zero-field parabolic-like bands scale nearly linearly with field $E_n^{\mathrm{c,v}} \propto \pm\sqrt{n(n+1)}B_0$. More precisely, they are close to be linearly dependent for the lower-energy states or the weaker field only, but involved as a combination of $\sqrt{B_0}$ and $B_0$ elsewhere. The absence of simple $B_0$ dependence can be easily inferred that the corresponding zero-field subbands are out of the parabolic band region. Besides, $E^{\mathrm{c,v}}(n)$ eventually fall to $E_{\mathrm{F}}$ in the limit of low field, which is similar to the monolayers.

Each Landau level is composed of four degenerate states with similar characteristics. At the $\Gamma$ point ($k_x = k_y = 0$), their wave functions are respectively located around $x = 1/6$, $1/3$, $2/3$, and $5/6$ of extended unit cell. Those of $x = 1/6$ and $n^{\mathrm{c,v}} \leq 5$ at 5 T are depicted in Fig. 2. In the case of monolayer graphene, wave function is composed of two inequivalent sublattices ($A_N$ and $B_N$). Each curve can be approximated by the product of the Hermite polynomial of order $n$ and the Gaussian function. The node number is $n$ for $A_N$ atoms with respect to $n - 1$ for $B_N$ atoms. Those of $A_N$-sites are chosen to label the quantum index $n^{\mathrm{c,v}}$ of Landau levels. All Landau levels are contributed almost equally by $A_N$- and $B_N$-sublattices, except for the $n = 0$ level by $A_N$ only. The distribution widths correspond to the magnetic lengths; they broaden with the increment of field stregth or Landau energy.

With regard to the Landau wave functions in bilayer graphene, they consist of four sublattices, $A_N^1$, $B_N^1$, $A_N^2$, and $B_N^2$, as shown in Figs. 2(c)–2(f). The node number between inequivalent atomic sites is $A_N^1 : B_N^1 : A_N^2 : B_N^2 =$

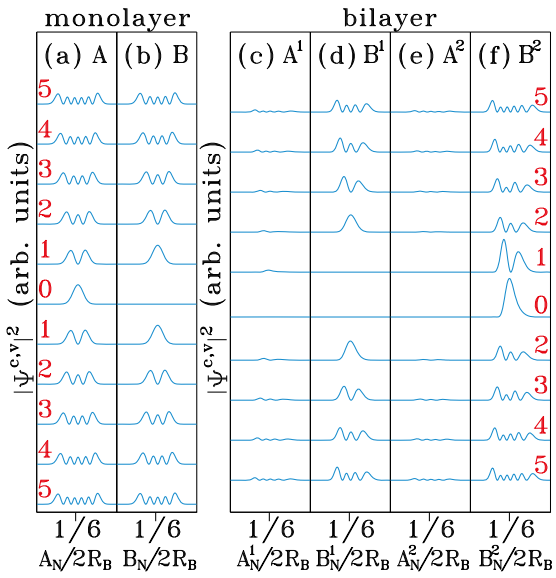


**Fig. 2.** (Color online) The wave functions of Landau levels with $n^{c,v} \leq 5$ at $B_0 = 5\,\mathrm{T}$. (a) $A_N$- and (b) $B_N$-sublattices for monolayers, and (c) $A^1_N$-, (d) $B^1_N$-, (e) $A^2_N$-, and (f) $B^2_N$-sublattices for bilayers; curves from bottom to top corresponding to state energies in sequence.

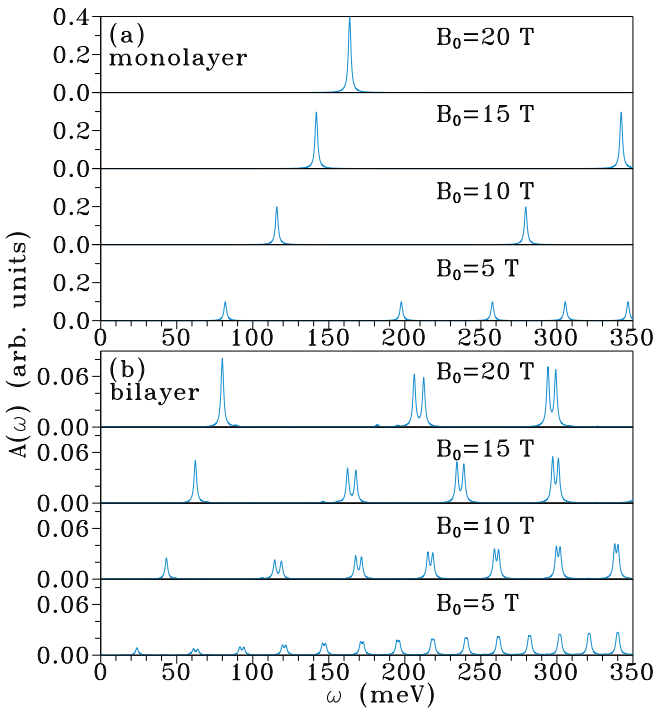


**Fig. 3.** (Color online) Optical absorption spectra of (a) monolayer and (b) bilayer graphene at 20, 15, 10, and 5 T.

$n-1 : n-2 : n-1 : n$ for $n^{c,v} \geq 2$. And the two lowest states ($n^c = 0$, $n^v = 1$) are almost provided by the $B^2_N$ atoms only. Since wave functions are mainly dominated by the $B^2_N$ atoms, the node numbers of $B^2_N$ are adopted to define the quantum index of Landau levels, $n^{c,v}$. With the increment of state energy or $n^{c,v}$, the minor $A_{1,2}$ sites would gradually raise their proportion in the entire wave function. Except for the level index definition, wave function is also an essential physical quantity that gives access to further transport and excitation properties.

The magneto-optical response is governed by transitions between Landau levels. The low-frequency spectra are illustrated in Fig. 3 for monolayer and bilayer graphene. The optical transition rate is qualitatively estimated by the velocity matrix elements, as well as the product of initial- and final-state wave functions, as depicted in eq. (2). In particular, the dominant contributions of velocity elements to optical excitations are due to the terms of in-plane hopping $\gamma_0$. That is, the way the wave function distributes between the same layered $A_N$- and $B_N$-subblattices enables to determine the absorption rate. In accordance with the orthogonal relation of Hermite polynomials, transitions are permitted only if the two subblattices behave same node number. For monolayer Landau levels, the node number of $A_N$ and $B_N$ steadily differ by one; accordingly, the selection rule is concluded to be $\Delta n = n^c - n^v = \pm 1$. In Fig. 3(a), the $i$th prominent peak is recognized as transitions of $n^v = i - 1 \to n^c = i$ and $n^v = i \to n^c = i - 1$. All peaks are equal in intensity since each Landau wave function is contributed almost equally by $A_N$- and $B_N$-sublattices. The rising $B_0$ would enhance the Landau degeneracy and thus the spectral intensity.

The bilayer spectra appear to be denser and richer in contrast to monolayers, as illustrated in Fig. 3(b). The intensity of these peaks is evidently suppressed and mutually non-uniform, which can also be explained by the wave function distribution. Due to the difference in atomic chemical environment, wave functions are strongly (weakly) localized on the $B^{1,2}_N$- ($A^{1,2}_N$-) sublattices. The absorption rate is determined by the product of major $B^1_N$ ($B^2_N$) sites and minor $A^1_N$ ($A^2_N$) sites, which qualitatively results in the overall weaker intensity. Bisides, the minor sites $A^{1,2}_N$ are gradually developed for higher energy levels, which can adequately elucidate the progressive growth of intensity with photon energy. Most pronounced peaks are paired together as a result of the break-down of electron–hole symmetry. Both the $\gamma_4$ and $\gamma_6$ are responsible for this electron–hole asymmetry. For the $i$th pair, the lower and higher peaks are recognized as transitions of $n^v = i + 2 \to n^c = i + 1$ and $n^v = i + 1 \to n^c = i + 2$, respectively. The energy difference in each pair becomes smaller in higher energy region or at weaker field. Whether these double peaks are observable in experiments closely relate to the broadening parameter $\Gamma$, which might be impacted by the temperature, defect scattering and other many-body effects. In addition, the threshold absorption peak involves transition $n^v = 2 \to n^c = 1$ only because of the absence of $n^c_1 = 0$, $n^v_1 = 1$ levels. The node numbers between sublattices are $A^1_N : B^1_N : A^2_N : B^2_N = n + 1 : n : n + 1 : n + 2$ and the level index is defined by the $B^2_N$ site. Hence, the selection rules for the dipole-allowed transitions are concluded to be $\Delta n = \pm 1$, which is intriguingly identical to that in monolayers.

The field evolution of absorption lines is plotted in Fig. 4. The absorption frequencies nearly scale as $\sqrt{B_0}$ in monolayers but $B_0$ in bilayers. This distinct signature of field dependence can be extrapolated from the $B_0 = 0$ energy dispersions in the vicinity of $K$-point, linear in monolayers but parabolic in bilayers.[20,21] Nevertheless, these absorption lines are neither $\sqrt{B_0}$ nor $B_0$ dependence in the stronger field or higher energy region. They eventually fall off to zero in the low-field limit. The spacings between absorption lines

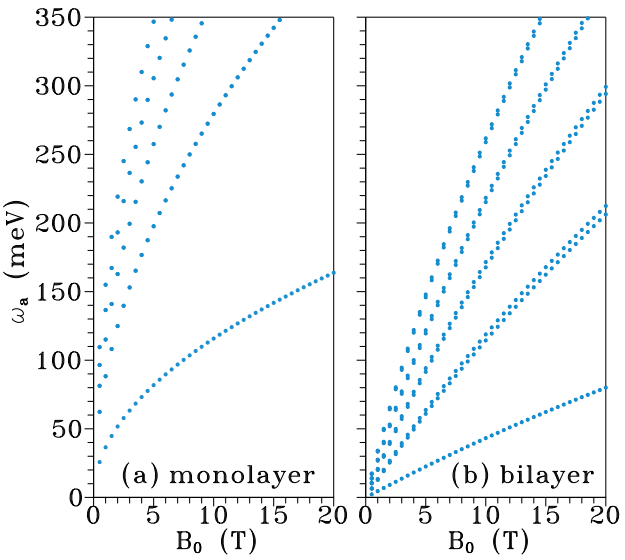


**Fig. 4.** (Color online) The first five $B_0$-dependent absorption frequencies for (a) monolayer and (b) bilayer graphene.

correlate to $\gamma_0$ in monolayers, but involve all atomic hoppings $(\gamma_0, \gamma_1, \gamma_3, \gamma_4, \gamma_6)$ in bilayers.

The calculations in the framework of Peierls tight-binding model are feasible for $\pi$-electron associated Landau levels since they take account of the magnetic field and interlayer interactions simultaneously. Compared to a flux quantum, the field strength available nowadays in laboratories is extremely small; hence, the field acts as the quantization of zero-field states with approximate energy into dispersionless Landau states. The atomic hoppings between layers essentially alter the two-dimensional subbands and consequently the quantized Landau levels at finite field. All specific hopping parameters play significant roles in the Landau level structures. Furthermore, the distribution over the sublattices provides a direct way to conclude the optical selection rules and the absorption rate. The influences of interlayer interactions on the electronic and optical properties would be confirmed by the magnetoabsorption spectroscopy.[12–16] Also, the numerical method developed in this work can be expanded to other graphene layers and other physical properties.

## 4. Conclusions

The interlayer interactions in bilayers significantly modify the quantized Landau levels and thus the inter-Landau-level optical excitations. The absorption lines in monolayers are approximated as square-root dependent on field, but are switched into nearly linear in bilayers. A close inspection of wave function distributions provides a intuitive way to resolve the specific selection rules and energy-dependent absorption rates. The electron–hole asymmetry results in the double-peaked absorptions. The spectral characteristics in this work would be beneficial in identifying the measurements on few-layer graphene sheets.

## Acknowledgment

This work was supported by the NSC and NCTS (South) of Taiwan, under the grant No. NSC 97-2112-M-110-001-MY2 and NSC 98-2112-M-006-013-MY4.

1) K. S. Novoselov, A. K. Geim, S. V. Morozov, D. Jiang, Y. Zhang, S. V. Dubonos, I. V. Grigorieva, and A. A. Firsov: Science **306** (2004) 666.
2) C. Berger, Z. Song, X. Li, X. Wu, N. Brown, C. Naud, D. Mayou, T. Li, J. Hass, A. N. Marchenkov, E. H. Conrad, P. N. First, and W. A. de Heer: Science **312** (2006) 1191.
3) T. Ohta, A. Bostwick, T. Seller, K. Horn, and E. Rotenberg: Science **313** (2006) 951.
4) T. Ohta, A. Bostwick, J. L. McChesney, T. Seyller, K. Horn, and E. Rotenberg: Phys. Rev. Lett. **98** (2007) 206802.
5) K. S. Novoselov, E. McCann, S. V. Morozov, V. I. Fal'ko, M. I. Katsnelson, U. Zeitler, D. Jiang, F. Schedin, and A. K. Geim: Nat. Phys. **2** (2006) 177.
6) K. S. Novoselov, A. K. Geim, S. V. Morozov, D. Jiang, M. I. Katsnelson, I. V. Grigorieva, S. V. Dubonos, and A. A. Firsov: Nature **438** (2005) 197.
7) Y. Zhang, Y. W. Tan, H. L. Stormer, and P. Kim: Nature **438** (2005) 201.
8) A. J. M. Giesbers, U. Zeitler, M. I. Katsnelson, L. A. Ponomarenko, T. M. Mohiuddin, and J. C. Maan: Phys. Rev. Lett. **99** (2007) 206803.
9) J. G. Checkelsky, L. Li, and N. P. Ong: Phys. Rev. Lett. **100** (2008) 206801.
10) B. E. Feldman, J. Martin, and A. Yacoby: Nat. Phys. **5** (2009) 889.
11) G. Li and E. Y. Andrei: Nat. Phys. **3** (2007) 623.
12) R. S. Deacon, K. C. Chuang, R. J. Nicholas, K. S. Novoselov, and A. K. Geim: Phys. Rev. B **76** (2007) 081406.
13) K.-C. Chuang, A. M. R. Baker, and R. J. Nicholas: Phys. Rev. B **80** (2009) 161410(R).
14) Z. Jiang, E. A. Henriksen, L. C. Tung, Y. J. Wang, M. E. Schwartz, M. Y. Han, P. Kim, and H. L. Stormer: Phys. Rev. Lett. **98** (2007) 197403.
15) M. Orlita, C. Faugeras, G. Martinez, D. K. Maude, M. L. Sadowski, and M. Potemski: Phys. Rev. Lett. **100** (2008) 136403.
16) M. L. Sadowski, G. Martinez, M. Potemski, C. Berger, and W. A. de Heer: Phys. Rev. Lett. **97** (2006) 266405.
17) D. S. L. Abergel and V. I. Fal'ko: Phys. Rev. B **75** (2007) 155430.
18) M. Koshino and T. Ando: Phys. Rev. B **77** (2008) 115313.
19) C. P. Chang, C. L. Lu, F. L. Shyu, R. B. Chen, Y. K. Fang, and M. F. Lin: Carbon **42** (2004) 2975.
20) C. P. Chang, C. L. Lu, F. L. Shyu, R. B. Chen, Y. C. Huang, and M. F. Lin: Carbon **43** (2005) 1424.
21) J. H. Ho, Y. H. Lai, Y. H. Chiu, and M. F. Lin: Nanotechnology **19** (2008) 035712.
22) For details of the geometric configuration and the Peierls tight-binding calculation of bilayer Bernal graphene, see Y. H. Lai, J. H. Ho, C. P. Chang, and M. F. Lin: Phys. Rev. B **77** (2008) 085426.
23) J. M. Luttinger: Phys. Rev. **84** (1951) 814.
24) K. Nakao: J. Phys. Soc. Jpn. **40** (1976) 761.
25) B. Partoens and F. M. Peeters: Phys. Rev. B **74** (2006) 075404.
26) G. D. Mahan: *Many-Particle Physics* (Plenum, New York, 1990).
27) L. G. Johnson and G. Dresselhaus: Phys. Rev. B **7** (1973) 2275.
28) M. F. Lin and K. W. K. Shung: Phys. Rev. B **50** (1994) 17744.